

## Field-emission Properties of Ni-C Nanocomposite Films

A.V. Arkhipov, P.G. Gabdullin, M.V. Mishin, V.S. Protopopova, S.I. Krel, D.E. Drobinin, N.M. Gnuchev\*

Peter the Great St.-Petersburg Polytechnic University, 29, Politekhnicheskaya st., 195251 St.-Petersburg, Russia

(Received 15 May 2016; published online 21 June 2016)

Field-emission properties of Ni-C nanocomposite thin films were experimentally studied. The films were deposited at Si substrates using CVD technique with a metalloorganic precursor and were composed by nm-scale grains of metallic Ni bounded with a carbonic weakly-conducting matrix. In the samples with lower effective thickness, the Ni particles were separated from each other. Such films showed capability of facilitated emission with threshold field values as low as a few V/ $\mu\text{m}$ . Thicker coating samples, with metallic particle merged in a conductive layer, required annealing at 470-600 °C in vacuum to produce low-field emission current. The observed emission behavior agrees with the previously proposed model considering low-field emission from nanostructured carbonic materials as a multi-stage process involving generation of hot electrons at interface boundaries.

**Keywords:** Field electron emission, Nanocomposite, Thin films, Carbon materials.

DOI: [10.21272/jnep.8\(2\).02058](https://doi.org/10.21272/jnep.8(2).02058)

PACS numbers: 79.70.+q, 79.60.Jv,  
81.05.uj, 81.07.-b

### 1. INTRODUCTION

The traditional design of field-emission cathodes is based on achievement of very high field enhancement at point areas of tungsten needles or carbon nanotubes. Though, this approach also implies concentration of all destructing factors at the emitter tips, which limits its lifetime or extracted current or both. At the same time, the possibility to obtain low-field cold electron emission from geometrically smooth surfaces had been recently demonstrated with different nanostructured refractory materials, mostly nanocarbons [1-9]. The precise mechanism of the emission facilitation in many cases remains unclear, but it is usually associated with nano-scale heterogeneity of the efficient emitters [7-9]. Work-function mismatch between adjacent nanodomains as well as partial penetration of the external field in emitter material and its concentration at interface boundaries can create beneficiary conditions for generation of hot electrons. Moreover, the hot electron energy relaxation in nanocrystals can be less efficient due to so-called "bottleneck effect" suppressing interaction between electrons and phonons. The hypothesis explaining the low-field emission phenomenon by combination of these factors had been previously proposed [10-12] for purely carbon heterogeneous ( $sp^2/sp^3$ ) structures. Yet, it can be also applied to any composite material or film composed by alternating conductive and dielectric nanosized domains. In this work, we studied emission properties of a product of joint deposition of carbon and nickel.

### 2. EXPERIMENTAL

The film samples were deposited at  $\sim 1\text{ cm}^2$  square substrates cut from standard  $n$ -type Si wafers. The deposition process (metal-organic chemical vapor deposition, MOCVD) was carried out in a hot-wall horizontal low-pressure tube silica reactor at temperatures 350-650 °C. The gas mixture included a metalloorganic

component ((EtCp) $_2$ Ni, or bis-(ethylcyclopentadienyl) nickel), hydrogen and argon, the latter serving as the buffer gas. Typical values of their partial pressures were 75, 210 and 545 Pa, respectively. Detailed description of the deposition technology may be found elsewhere [13].

Effective thickness of the deposited Ni layer was estimated by the characteristic line intensity in X-ray fluorescence spectra measured with the Spectroscan MAX-GV spectrometer. Scanning electron microscope (SEM) Supra 55 VP was used to determine the sample films' topography. Its x-ray detector was selectively sensitive to the Ni component of the deposit, which allowed us to visualize its distribution in the carbon matrix (Fig. 1).

Field-emission properties of the samples were examined in a special set-up described in more detail in [10-12]. The extracting electric field was applied in a planar gap, 0.5-0.6 mm in width, between the sample and a cylindrical anode. The emission tests were performed in vacuum, with residual gas pressure  $10^{-6}$ - $10^{-7}$  Torr.

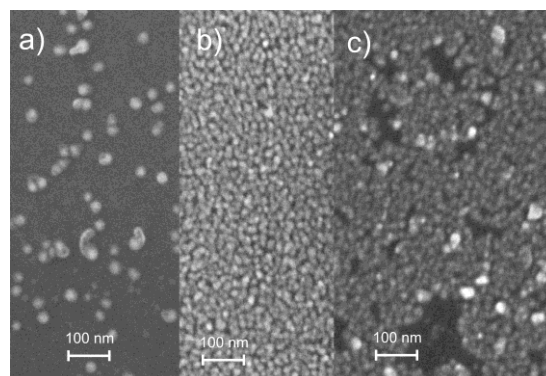


**Fig. 1** – SEM images of two Ni-C composite samples: a) sample A2; b) sample A3; c) sample A3 after annealing and emission tests

\* [Gnuchev.nm@spbstu.ru](mailto:Gnuchev.nm@spbstu.ru)

Sample heating for its degassing or annealing up to approximately 900 °C was possible *in situ*, with vacuum conditions maintained in the specified range.

### 3. RESULTS AND DISCUSSION

#### 3.1 Film Morphology

The film topography studies revealed that at early stages of deposition its Ni component had the form of separate nanoparticles covering only a small part of the substrate area (Fig. 1a). Later, the particles grew in size and number and eventually formed a complete layer (Fig. 1b). Further deposition did not visibly affect the surface topography, while the growth of the effective Ni layer thickness continued. The deposition rate was determined by the substrate temperature and partial pressures of the gas mixture. The carbonic component of the film (practically invisible in the showed SEM images) had the forms of the amorphous carbon and carbide shells of the Ni particles.

#### 3.2 Emission Properties

Emission properties of the studied composite samples showed reproducible correlation with film morphology. They were distinctly different for films with Ni particles forming at least one full monolayer (completely covering the substrate) and films of lower effective Ni layer thickness where the metallic particles were separated.

##### 3.2.1 Sub-monolayer Films

Table 1 gives the main parameters of deposition process and morphology for three samples with the quantity of Ni insufficient for the metallic particles to form a complete layer. Morphologically, the main difference between these samples consisted in the particles' mean size. This parameter correlates with deposition temperature and presumably determines the observed difference in emission properties.

**Table 1** – Properties of sub-monolayer films

Sample	Deposition temp., °C	Deposition time, min	Mean size of Ni grains, nm	Low-field emission (before / after annealing)
A1	390	60	11	+ /
A2	410	60	20	++ /
B1	490	10	30	- / +

All three samples were capable of low-field emission, even though in different degrees. The best emission properties were demonstrated by sample A2 with the mean size of Ni grains ~20 nm. Its SEM image is showed in Fig. 1a. The emission started without any special activation procedures, such as high-temperature annealing. The *I-V* characteristics had exponential shape and relatively weak temperature dependency, which confirms tunneling nature of the current. The threshold field (necessary for extraction of 10 nA) was close to 2 V/μm, i.e. had a typical value observed in our previous studies for various forms of nanostructured carbon [10-12].

Sample A1 with smaller Ni particles (mean size ~11 nm) also showed low-field emission in the “as grown” condition, though the threshold field was higher – approximately 4 V/μm. Sample B1 with the largest Ni particles (~30 nm) demonstrated the worst emission properties. The current appeared only after annealing, even if at a relatively low temperature (380 °C). The best threshold field for this sample amounted to ~7 V/μm, and its emission properties rapidly deteriorated.

Certainly, the experiment data obtained with only three composite samples cannot give us a statistically significant basis for any general statements. Yet notably, the data are in good agreement with the emission model [10-12] that predicted existence of an optimal size of insulated conductive domains at the emitter surface. The mean size of Ni particles of the best emitter (~20 nm) fits well with the expected optimum value, determined as the largest size of a domain where the “phonon bottleneck” phenomenon can efficiently suppress hot electron energy relaxation.

##### 3.2.2 Full-monolayer Films

Three samples of composite films with the Ni component forming approximately one full monolayer of nanoparticles (Fig. 1b) were fabricated using different combinations of deposition time and substrate temperature (Table 2).

**Table 2** – Properties of full-monolayer films

Sample	Deposition temp., °C	Deposition time, min	Low-field emission (before / after annealing)
A4	450	60	- / -
B2	530	10	- / +
A3	570	5	- / +

Sample A4 fabricated at the lowest temperature did not show the capability of low-field emission, either in the “as grown” state or after attempts of activation by annealing at temperatures up to 470 °C.

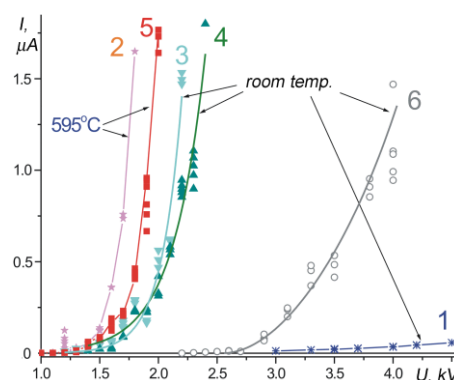


**Fig. 2** – Emission characteristics of sample A2 measured at different temperatures in the course of activation treatment

Both other full-monolayer samples (A3 and B2) acquired the property of low-field emission after annealing. The best achieved threshold field values for them were 3.5 and 2.5 V/μm, respectively. Effect of annealing on emission properties of sample B2 is illustrated in Fig. 2 by a set of emission *I-V* plots. The sample yielded

some emission current even in the “as-grown” condition at room temperature (curve 1), but heating to 595 °C led to substantial activation of emission (curve 2). Cooling to the room temperature resulted in reduction of emission current (curve 3), though not very deep – approximately equivalent to 20 % field decrease. The annealing had a long-term activating effect on emission, remaining after further cycles of heating and cooling (curves 4, 5). An experiment on extraction of a larger current led to certain deterioration and stabilization of its emission properties (curve 6), which is usually associated with elimination of a few dominating emission sites.

The observed emission behavior of the films representing full monolayers of Ni grains in carbon matrix agrees with the previously discussed model. Poor emission properties demonstrated by the “as-grown” samples can be explained by good electric conductivity of the films composed by merged metal grains, preventing penetration of the field to internal domain junctions. Annealing can reduce conductivity of the film and electrically insulate the particles it comprises. One of possible mechanism of this effect may consist in formation of carbide shells around the metallic particles. The grain contacts can also be destroyed by the carbon matrix fracturing caused by its non-uniform graphitization with a dramatic (by ~ 50 %) change of specific volume. In the case of sample A3, a partial destruction of the film was visible in SEM images made after the emission tests (Fig. 1c). Poor emission properties of sample A4 can be attributed to insufficient temperature of its annealing.

### 3.2.3 Thick Film

One of the tested composite films (sample B3) had the effective Ni layer thickness (determined from x-ray fluorescence data) as large as ~ 200 nm. The SEM images confirmed that, like in all other cases, its metallic component was represented by nm-scale spherical particles. The number of their monolayers in the film can be estimated as  $\geq 10$ . The duration of the deposition process performed at 570 °C was 30 min. The film yielded emission current after annealing at 750 °C. The best threshold field was 4.5 V/ $\mu\text{m}$ , which is close to this parameter for the other composite samples.

A distinguishing feature of the multi-layer film consisted in steeper temperature dependence of its emission characteristics (Fig. 3a). Reduction of the applied field by 20 % approximately corresponded to 300 °C temperature decrease, which means ~ 2 times greater temperature effect than that for thinner films (Fig. 2).

One of possible explanations of the observed temperature dependency may consist in the mixed, thermionic-field (T-F) emission nature. To check this hypothesis, we can apply the mathematical apparatus developed for the T-F emission [14] to the data presented in Fig. 3a. In Fig. 3b they are re-plotted in Shottky coordinates  $\ln I = f(E^{1/2})$ . At the high-field part of the plot, the data approximately fit straight lines, as it is predicted by the T-F emission theory. At the low-field part, the curves are bended. The direction of the knee is opposite to the one normally present in T-F emission plots (for instance, in [15]), where it separates regimes of saturation and space-charge limited current. In our

case, the slope angles in the low-field area are reduced in comparison with the rest of the plot.

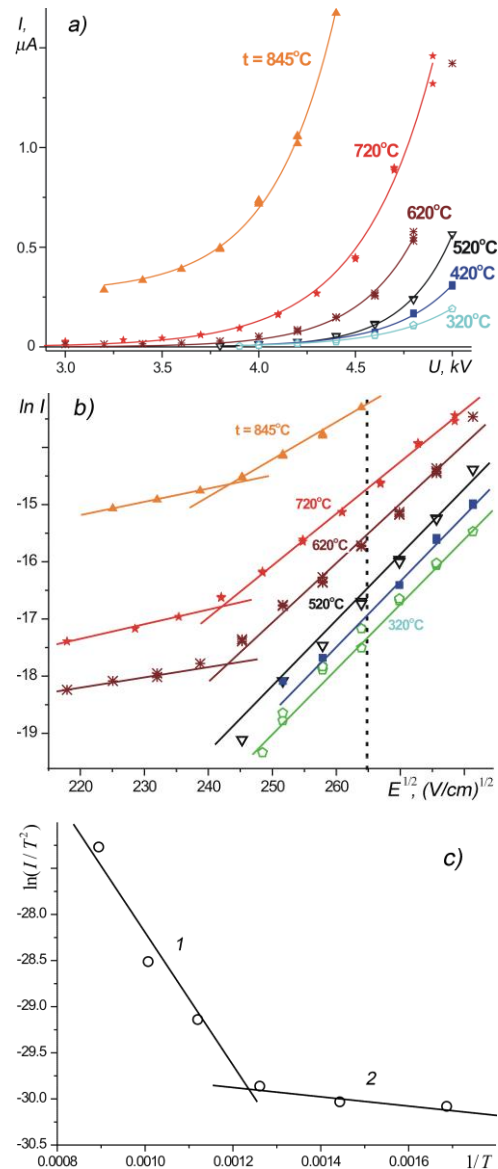


**Fig. 3** – Emission characteristics of sample B3 measured at different temperatures plotted in ordinary  $I$ - $V$  (a), Shottky (b) and Richardson (c) coordinates

The next step in the standard data treatment algorithm [15] would consist in extrapolation of the linear trends of the Shottky graphs in the saturation (high-field) area to the zero field and plotting of the obtained current values ( $I$ ) against the temperature ( $T$ ) in Richardson coordinates  $\ln(I/T^2) = f(1/T)$ . Regretfully, this procedure was hardly applicable to the data of Fig. 3b because of insufficient field variation range for a correct extrapolation. Therefore, the data plotted in Fig. 3c in Richardson coordinates refer to the non-zero field value indicated in Fig. 3b with the vertical dotted line. The resulting Richardson plot (Fig. 3c) was far from linear. Its approximation with two linear segments showed in the graph could describe a two-component emitting surface (as it had been done, for instance, in [16]), with Richardson’s workfunction values 0.043 and 0.62 eV. Though, interpolation of the

data set with a smooth curve seems more appropriate, which gives us a continuous distribution of Richardson workfunction covering the previously indicated range.

Thus, interpretation of the temperature dependency of emission characteristics in terms of the T-F emission theory yields the implausible picture of a very inhomogeneous surface with some areas having workfunction as low as a few room-temperature  $kT$ . This picture contradicts to experimental facts (such as exponential shape of  $I$ - $V$  curves and/or wrong direction of the knee in the Shottky plots in Fig. 3b) as well as general considerations (this low workfunction can hardly be expected for a structure built of Si, Ni and C). Another objection originates from comparison with the one-monolayer samples having surface morphologically identical (or very similar) to the one of the thick film. The observed difference in their emission properties, including the difference in the thermal dependency of emission, is most probably associated with the additional internal layers of the composite. Thermal dependency of its resistivity can explain steeper thermal dependency of emission observed for the thicker film sample. In this case, the Richardson slope values determined by the above anal-

yses can be interpreted as the values of the activation energy of electric conduction through the composite. Its wide continuous distribution reflects disordered structure of the film and diversity of current paths. The weaker effect of temperature onto emission from the thinner films can also be associated with temperature-dependent electron transport to emission sites.

#### 4. CONCLUSIONS

As a whole, the results of the performed experiments are in good agreement with the multiple-barrier hot-electron emission model [10-12], describing the role of nanoparticles in emission facilitation as consisting in: 1) enhancement of the applied field at internal junctions to provide free energy for generation of hot electrons and 2) suppression the most efficient mechanism of hot electrons' relaxation leading to their lifetime increase. With regard to the studied Ni-C composite, the model predicted the existence of an optimal Ni grain size and worse emission properties of full merged layer of the grains in comparison with films comprised by isolated metallic particles.

#### Автоэмиссионные свойства пленок никель-углеродного нанокompозита

А.В. Архипов, П.Г. Габдуллин, М.В. Мишин, В.С. Протопопова, С.И. Крель, Д.Э. Дробинин, Н.М. Гнучев

Санкт-Петербургский политехнический университет Петра Великого, ул. Политехническая, 29, 195251 Санкт-Петербург, Россия

Были исследованы автоэмиссионные свойства тонких пленок никель-углеродного нанокompозита. Пленки наносились на кремниевые подложки методом химического осаждения с использованием металлорганического прекурсора. Их структура включала в себя наноразмерные зерна металлического никеля, связанные слабопроводящей углеродосодержащей матрицей. В случае покрытий малой эффективной толщины, частицы никеля были отделены друг от друга. Такие пленки демонстрировали способность к низковольтной эмиссии в полях с напряженностью от нескольких В/мкм. В более толстых покрытиях металлические частицы образовывали единый электропроводящий слой. В этом случае для наблюдения низковольтной эмиссии требовался отжиг образцов в вакууме при 470-600 °С. Наблюдавшиеся закономерности эмиссии согласуются с предлагавшейся ранее моделью, которая рассматривает низковольтную эмиссию из нанокompозитных материалов как многостадийный процесс с участием горячих электронов, образующихся на внутренних междоменных границах.

**Ключевые слова:** Автоэлектронная эмиссия, Нанокompозит, Тонкие пленки, Углерод.

#### REFERENCES

1. A. Okotrub, L. Bulusheva, A. Gusel'nikov, V. Kuznetsov, Yu. Butenko, *Carbon* **42**, 1099 (2004).
2. Z. Shpilman, Sh. Michaelson, R. Kalish, A. Hoffman, *Diam. Relat. Mater.* **15**, 846 (2006).
3. O.S. Panwar, N. Rupesinghe, G.A.J. Amaratunga, *J. Vac. Sci. Technol. B* **26**, 566 (2008).
4. K. Uppireddi, B.R. Weiner, G. Morell, *J. Vac. Sci. Technol. B* **28**, 1202 (2010).
5. P.-C. Huang, W.-C. Shih, H.-C. Chen, I.-N. Lin, *J. Appl. Phys.* **109**, 084309 (2011).
6. K. Nose, R. Fujita, M. Kamiko, Y. Mitsuda, *J. Vac. Sci. Technol. B* **30**, 011204 (2012).
7. A. Karabutov, V. Frolov, V. Konov, V. Ralchenko, S. Gordeev, P. Belobrov, *J. Vac. Sci. Technol. B* **19**, 965 (2001).
8. A.N. Obraztsov, Al.A. Zakhidov, *Diam. Relat. Mater.* **13**, 1044 (2004).
9. L.D. Filip, M. Palumbo, J.D. Carey, S.R.P. Silva, *Phys. Rev. B* **79**, 245429 (2009).
10. A.V. Arkhipov, P.G. Gabdullin, M.V. Mishin, *Fuller. Nanotub. Car. N.* **19** No 1-2, 86 (2011).
11. A.V. Arkhipov, P.G. Gabdullin, N.M. Gnuchev, A.Yu. Emel'yanov, S.I. Krel', *Tech. Phys. Lett.* **40**, 1065 (2014).
12. A. Arkhipov, S. Davydov, P. Gabdullin, N. Gnuchev, A. Kravchik, S. Krel', *J. Nanomater.* **2014**, 190232 (2014).
13. S.E. Alexandrov, V.S. Protopopova, *J. Nanosci. Nanotechnol.* **11**, 8259 (2011).
14. L.N. Dobretsov, M.V. Gomoyunova, *Emission Electronics* (Jerusalem: Isr. Prog. Sci. Trans.: 1971).
15. Feng Jin, Yan Liu, C.M. Day, *Appl. Phys. Lett.* **90**, 143114 (2007).
16. I.S. Altman, P.V. Pikhitsa, M. Choi, *J. Appl. Phys.* **96**, 3491 (2004).